Proceedings of Advanced
Intelligent Mechatronics
AIM'97, Tokyo,Japan,1997

Vision-Based Impedance Control for Robot Manipulators

Toshio Tsuji, Hiromasa Akamatsu, Michio Hatagi and Makoto Kaneko
Industrial and Systems Engineering
Hiroshima University
1-4-1, Kagamiyama, Higashi-Hiroshima 739, JAPAN
E-Mail : tsuji@huis.hiroshima-u.ac.jp

Abstract— **This paper proposes an impedance control method that can regulate a virtual impedance between an end-point of a robot manipulator and external objects using visual information. The conventional impedance control methods are not useful for some cases where no interaction force between the arm and its environment occurs, although it is one of the most effective control method for manipulators in contact with the environment. Using the proposed method, we can control the manipulator motion based on the virtual impedance before contact with the objects. Validity of the proposed method is verified through experiments using a direct-drive robot.**

I Introduction

Impedance control is a method to regulate a mechanical impedance of an end-effector of a robot manipulator in a desired value according to a given task. It can specify desirable response of the end-effector for an external force. Hogan [1] invented a method to control the end-effector impedance of a manipulator based on measured position, velocity and force of the end-effector. Then many studies have been conducted such as a realization technique without use of an inverse of a Jacobian matrix [2], without use of a force sensor [3] and stability analysis for contact motion [4]. The impedance control is one of the most important framework to control the interaction between the manipulators and the environment.

In some cases, however, occurrence of an interaction force between a manipulator and its environment should be carefully considered. For example, when the end-effector handles a fragile object, an approaching velocity of the end-effector should be decreased before coming into contact with the object in order to prevent a large impact force. Also in some environments including obstacles, the interaction force between the obstacle and the manipulator should be avoided. Under the conventional impedance control, it is difficult to cope effectively with such situations, since no external force is exerted until the end-effector contacts with objects.

0-7803-4089-9/97/$10.00 c 1997 IEEE

On the other hand, vision-based control for robot manipulators has been actively studied in recent years [5, 6, 7], where the robot is controlled according to visual information on the task space. Based on the framework of the vision-based control, Castano and Hutchinson [8] proposed a concept of a visual compliance. This method can constrain the end-effector motion on a virtual task plane based on a hybrid control using the visual sensor information from a camera system and the internal joint angle sensor information from an encoder at each joint of the manipulator. However, it does not control impedance characteristics itself based on visual information.

As impedance control using visual information, only a few methods have been proposed so far. Arai, Ohta and Suzuki [9] proposed a concept of a virtual impedance for motion planing of multiple mobile robots. In their method, the virtual impedances among the robots, the goal and the obstacles are defined, and virtual forces resulted from the virtual impedances are utilized in order to achieve coordinated control of the multiple mobile robots. Nakabo et al. [10] proposed a concept of a visual impedance and showed that the movement of the end-effector can be modified in real time (remarkably, less than 1 ms sampling time) by using the visual impedance between the end-effector and the object. We also proposed a vision-based impedance control [11] using a virtual impedance, which can control a virtual impedance between the end-effector and the object as well as the end-effector's impedance.

In this paper, we apply the vision-based impedance control to a robot manipulator and discuss how the virtual impedance parameters can be designed with consideration of the overall control property of the system. The proposed method can control the virtual impedance between the object and the end-effector, so that the relative end-effector motion to the object can be controlled without contact through a virtual external force generated by the virtual impedance and visual sensor information. Finally, experiments using a direct-drive robot are performed in order to make clear the distinctive feature of the proposed method.

II Impedance Control

In general, a motion equation of an m-joint manipulator can be expressed as follows

$$M(\theta)\ddot{\theta} + h(\theta,\dot{\theta}) + g(\theta) = \tau + J^T(\theta)F_{ext}, \qquad (1)$$

where $F_{ext} \in \Re^l$ is the external force exerted on the end-effector; $\theta \in \Re^m$ is the joint angle vector; $M(\theta) \in \Re^{m\times m}$is the non-singular inertia matrix (hereafter denoted by M); $h(\theta,\dot{\theta}) \in \Re^m$ is the nonlinear term including the joint torque due to the centrifugal, Coriolis and friction forces; $g(\theta)$ is the joint torque due to gravity; $\tau \in \Re^m$ is the joint torque vector; $J(\theta) \in \Re^{l\times m}$ is the Jacobian matrix (hereafter denoted by J); and l is the dimension of the task space.

Now, the desired impedance of the end-effector is described by

$$M_e d\ddot{X} + B_e d\dot{X} + K_e dX = F_{ext}, \qquad (2)$$

where $M_e, B_e, K_e \in \Re^{l\times l}$ are the desired inertia, viscosity and stiffness matrices of the end-effector, respectively; and $dX = X - X_d \in \Re^l$ is the displacement vector between the current end-effector position X and the desired one (namely, the equilibrium position of the end-effector) X_d.

In this paper, we adopt the impedance control law without calculation of the inverse Jacobian matrix presented in [2]:

$$\tau = \tau_{effector} + \tau_{comp}, \qquad (3)$$

$$\tau_{effector} = -J^T[M_x(\theta)\{M_e^{-1}(K_e dX + B_e d\dot{x} + \dot{J}\dot{\theta} - \ddot{X}_d\} + \{I - M_x(\theta)M_e^{-1}\}F_{ext}], \qquad (4)$$

$$\tau_{comp} = (\bar{J}J)^T\hat{h}(\theta,\dot{\theta}) + \hat{g}(\theta), \qquad (5)$$

where $M_x(\theta) = (J\hat{M}^{-1}J^T)^{-1} \in \Re^{l\times l}$ is the operational space kinetic energy matrix [12, 13]; $\bar{J} = \hat{M}^{-1}J^T M_x(\theta) \in \Re^{m\times l}$ is the generalized inverse of J weighted by $\hat{M}^{-1}$; $\tau_{effector} \in \Re^m$ is the joint torque vector needed to produce the desired end-effector impedance; I is the $l \times l$ identity matrix; $\tau_{comp} \in \Re^m$ is the joint torque vector for nonlinear compensation; and $\hat{h}(\theta,\dot{\theta})$, $\hat{g}(\theta)$ and $\hat{M}$ are the estimated values of $h(\theta,\dot{\theta})$, $g(\theta)$ and M. It is assumed that $\hat{h}(\theta,\dot{\theta}) = h(\theta,\dot{\theta})$, $\hat{g}(\theta) = g(\theta)$, $\hat{M} = M$, and the joint configuration θ is not in a singular posture.

III Vision-Based Impedance Control

Figure 1 shows a schematic representation of the proposed impedance control. Let us consider the case that an object approaches a manipulator. In order to consider the interaction between the end point of the arm and the object without contact, a virtual sphere with radius r is used, where center of the sphere is located on the end-point of the manipulator as shown in Fig. 1. Then, when the object comes into the interior of the

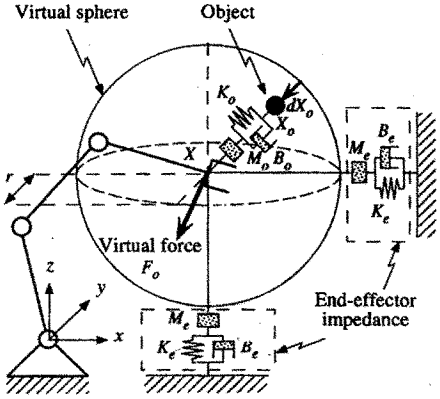

Figure 1: Schematic representation of a Vision-Based Impedance Control

virtual sphere, the normal vector from the surface of the sphere to the object is given as

$$dX_o = X_r - ra, \qquad (6)$$

where $X_r = X_o - X$ is the displacement vector from the end-point $X \in \Re^l$ to the object $X_o \in \Re^l$. Also the vector $a \in \Re^l$ is defined as

$$a = \begin{cases} \frac{X_r}{|X_r|} & (|X_r| \neq 0) \\ 0 & (|X_r| = 0) \end{cases}, \qquad (7)$$

where $|X_r|$ denotes the Euclidian norm of X_r. When the object is in the virtual sphere, $|X_r|$ is less than r.

Then the virtual impedance is considered between the object and the center of the virtual sphere as shown in Fig. 1, where M_o, B_o and K_o represent the virtual inertia, viscosity and stiffness matrices, respectively. Using the virtual impedance and the displacement vector dX_o, the virtual external force $F_o \in \Re^l$ exerted from the object to the end-point is defined as

$$F_o = \begin{cases} M_o d\ddot{X}_o + B_o d\dot{X}_o + K_o dX_o & (|X_r| < r) \\ 0 & (|X_r| \geq r) \end{cases}. \qquad (8)$$

It can be readily seen from (7) and (8) that F_o becomes zero when the object is not in the virtual sphere or the object exists at the center of the sphere.

The virtual external force F_o is directly incorporated in the motion equation of the end-effector (2):

$$M_e d\ddot{X} + B_e d\dot{X} + K_e dX = F_{ext} + F_o. \qquad (9)$$

Consequently, by revising (3) the vision-based impedance control law is given as

$$\tau = \tau_{effector} + \tau_{comp} + \tau_o. \qquad (10)$$

$$\tau_o = J^T F_o. \qquad (11)$$

Figure 2 shows the block diagram of the proposed impedance control. In addition to the end-effector

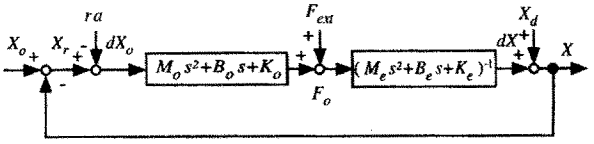

Figure 2: The block diagram of the vision-based impedance control

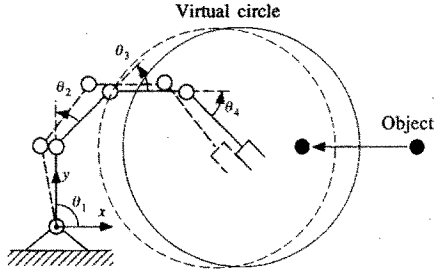

Figure 3: Avoidance of an object

impedance control that can regulate M_e, B_e, K_e according to the given task, the relative motion between the manipulator and its environment can be considered through the virtual impedance M_o, B_o, K_o using the vision-based impedance control.

IV Computer Simulation

Computer simulation using a four-joint planar manipulator shown in Fig. 3 was carried out. The parameters of each link of the manipulator are as follows: the length is 0.4 m, the mass 3.75 kg, the moment of inertia 0.8 kgm^2, and the center of mass of each link is at its middle point. The end-effector impedance of the manipulator is determined as M_e = diag.[1, 1] kg, B_e = diag.[20, 20] Ns/m, K_e = diag.[100, 100] N/m, and the desired end-effector position, i.e. the equilibrium position, is simply chosen as its initial position, where the initial posture of the manipulator is $\theta(0) = [\frac{\pi}{2}, -\frac{\pi}{4}, -\frac{\pi}{4}, -\frac{\pi}{4}]^T$ rad. The computation of the manipulator dynamics was performed by using the Appel's method [14], and the sampling time is 1 ms.

IV-A Application to object avoidance

Let us consider the manipulator close to the object. By using the conventional impedance control only, the manipulator cannot take any action for avoiding the object without the interaction force.

As the example of the vision-based impedance control, virtual circle is attached at the end-effector as shown in Fig. 3. The time histories of the end-effector trajectory $x(t)$ and the object trajectory $x_o(t)$ in the x direction are shown in Fig. 4, where the radius of the sphere is $r = 0.3$ m; and the virtual stiffness is changed as K_o = diag.[0, 0], diag.[50, 50], diag.[100, 100] N/m with constant inertia and viscosity M_o = diag.[0.5, 0.5] kg, B_o = diag.[10,10] Ns/m. The object is oscillating with the period of 2 s and the amplitude of 0.3 m in the direction of x axis as shown in Fig. 3. When the distance between the end-effector and the object is more than r, the end-effector does not move. However, when the object comes into the virtual circle, the end-effector is displaced in the direction opposite to the object. Also the trajectories of the end-effector reflects the stiffness between the end-effector and the object.

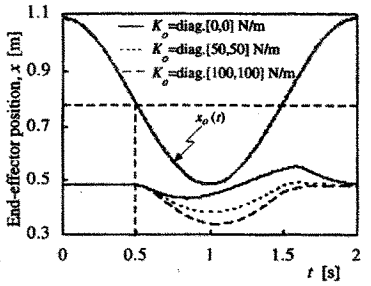

Figure 4: Change of the end-effector trajectories for the object under the proposed method

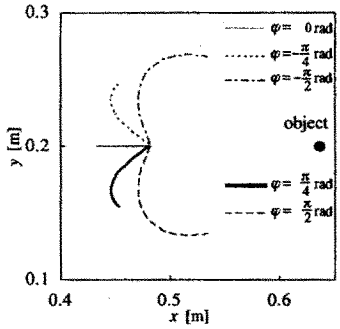

Figure 5: Control of the end-effector trajectories via the virtual impedance matrices

Next, the virtual impedance matrices M_o, B_o, K_o are changed as

$$\begin{aligned} M_o(\varphi) &= 0.5R(\varphi)\ \text{kg}, \\ B_o(\varphi) &= 10R(\varphi)\ \text{Ns/m}, \\ K_o(\varphi) &= 50R(\varphi)\ \text{N/m}, \\ R(\varphi) &= \begin{pmatrix} \cos\varphi & -\sin\varphi \\ \sin\varphi & \cos\varphi \end{pmatrix}, \end{aligned}$$

and the step response of the end-effector is examined, where the object is located at the position with a distance 0.15 m apart from the initial position of the end-effector in the direction of x axis. According to the rotation matrix $R(\varphi)$, the direction of the virtual external force is rotated with the angle φ in the counterclockwise direction from the direction of the vector dX_o.

Figure 5 shows the change of the step responses of the end-effector with the angle φ. The response of

the end-effector (namely, the amplitude and the direction) can be controlled by regulating the non-contact impedance matrices.

IV-B Virtual impedance parameters

As shown in Fig. 4, the dynamic response of the manipulator to the object's motion is highly depending on the virtual impedance as well as the end-point impedance.

The motion equation of the end-point of the manipulator can be derived by substituting (8) into (9) as follows:

$$M d\ddot{X} + B d\dot{X} + K dX = \tilde{F}, \tag{12}$$

$$\begin{aligned} \tilde{F} = F_{ext} &+ M_o\left(\ddot{X}_o - \ddot{X}_d - r\ddot{a}\right) \\ &+ B_o\left(\dot{X}_o - \dot{X}_d - r\dot{a}\right) \\ &+ K_o\left(X_o - X_d - ra\right), \end{aligned} \tag{13}$$

where $M = M_e + M_o$, $B = B_e + B_o$ and $K = K_e + K_o$. For simplicity, we assume that the vector a is constant. Then, we have

$$\frac{X(s)}{X_o(s)} = \left(Ms^2 + Bs + K\right)^{-1}\left(M_o s^2 + B_o s + K_o\right) \tag{14}$$

where $X(s)$, $X_o(s)$ denote the Laplace transform of $X(t)$, $X_o(t)$, respectively. Therefore we can see that the dynamic response of the end-point is determined by the sum of the virtual impedance and the end-point impedance. In Fig. 4, for example, the case of K_o=diag.[0, 0] N/m shown as the solid line results an overdamped response. Therefore, the end-point follows the object going further from the end-point, so that the large overshoot is observed after the object goes out of the virtual sphere.

The end-point impedance parameters M_e, B_e, K_e should be determined according to a task. Here, we discuss how the virtual impedance parameters can be designed with consideration of the overall system characteristics (14). For simplicity, let us consider the following positive definite matrices as the end-point impedance:

$$M_e = T^T \tilde{M}_e T, \tag{15}$$

$$B_e = T^T \tilde{B}_e T, \tag{16}$$

$$K_e = T^T \tilde{K}_e T, \tag{17}$$

where $T \in \Re^{l\times l}$ is the nonsingular matrix, each column of which corresponds to an eigenvector; and $\tilde{M}_e, \tilde{B}_e, \tilde{K}_e \in \Re^{l\times l}$ are the diagonal matrices, each diagonal element of which is an eigenvalue of the corresponding impedance matrices, respectively.

In this paper, we choose the following virtual impedance matrices:

$$M_o = T^T \tilde{M}_o T, \tag{18}$$

$$B_o = T^T \tilde{B}_o T, \tag{19}$$

$$K_o = T^T \tilde{K}_o T. \tag{20}$$

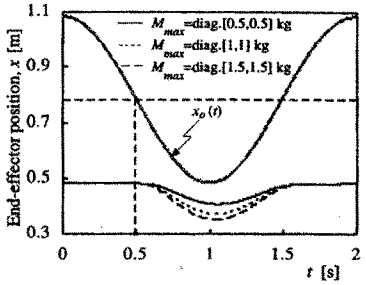

Figure 6: Change of the end-effector trajectories for the object, where $\zeta^{(i)} = 1$ and $\omega_n^{(i)} = 10$ rad/s $(i = 1, 2)$

Then, the problem is how to design the eigenvalues of the virtual impedance matrices. As an example, the eigenvalues of $\tilde{B}_o$ and $\tilde{K}_o$ are determined as follows:

$$\tilde{B}_o^{(i)} = 2\omega_n^{(i)}\zeta^{(i)}\left(\tilde{M}_e^{(i)} + \tilde{M}_o^{(i)}\right) - \tilde{B}_e^{(i)}, \tag{21}$$

$$\tilde{K}_o^{(i)} = \left(\omega_n^{(i)}\right)^2\left(\tilde{M}_e^{(i)} + \tilde{M}_o^{(i)}\right) - \tilde{K}_e^{(i)}, \tag{22}$$

where $\tilde{B}_o^{(i)}$, $\tilde{K}_o^{(i)}$ are the i-th diagonal elements of $\tilde{B}_o$, $\tilde{K}_o$, respectively; $\zeta^{(i)}$, $\omega_n^{(i)}$ are the damping ratio and the natural frequency for the corresponding degree of the freedom, respectively. It should be noted that the eigenvalues defined as (21) and (22) are not necessary to be positive, because the stability of the system is determined by the sum of the virtual impedance and the end-point impedance as (14).

For the i-th diagonal element of the virtual inertia M_o is also defined as

$$\tilde{M}_o^{(i)} = \frac{|dX_o|}{r} M_{max}^{(i)}, \tag{23}$$

where $M_{max}^{(i)}$ is the upper limit of the virtual inertia in the corresponding degree of the freedom. When the object comes into contact with the surface of the virtual sphere, the virtual inertia is automatically set to be small. As the object approaches the end-point, the virtual inertia becomes larger. Using (21), (22), (23), we can control the dynamic response of the end-point to the object motion according to the object position as well as the given end-point impedance.

Figure 6 shows an example of the simulation results using (21), (22), (23), where the upper limit of the virtual inertia $M_{max}^{(i)}$ are changed as $M_{max}^{(i)} = 0.5, 1.0, 1.5$ kg $(i = 1, 2)$. On the other hand, the constant damping ratio and the natural frequency are used: $\zeta^{(i)} = 1$ and $\omega_n^{(i)} = 10$ rad/s $(i = 1, 2)$. Other simulation conditions are the same as the ones used in Fig. 4. Note that the matrix T is the identity matrix, since the given end-point impedance matrices are diagonal. From the figure, it can be seen that the end-point returns to its initial position without overshoot as specified by the

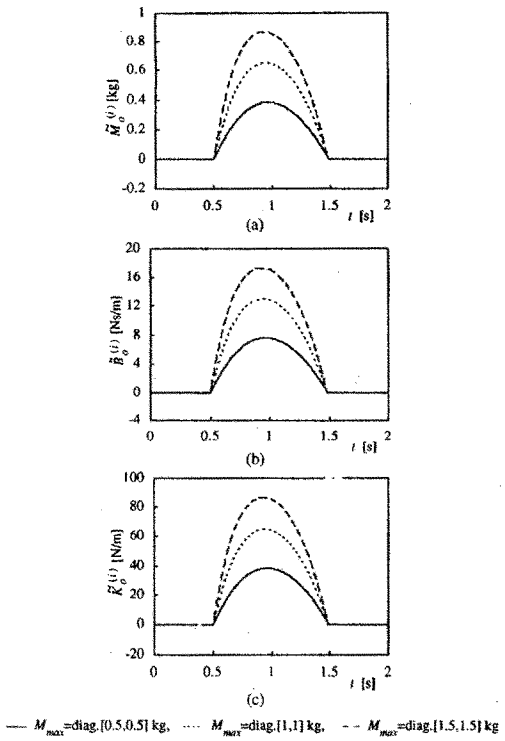

Figure 7: Time histories of the virtual impedance parameters

Table 1: Link parameters of the robot

	link 1	link 2	link 3
length (m)	0.25	0.25	0.125
mass (kg)	20.8	13.2	8.84
center of mass (m)	0.064	0.065	0.031
moment of inertia (kgm^2)	0.334	0.196	0.0851
joint friction (Nms/rad)	2.69	1.88	0.0634

damping ratio. The changes of the virtual impedance parameters are also shown in Fig. 7, where the parameters are adaptively regulated according to the object motion.

V Experiments

The experiment of the proposed impedance control was carried out using a direct-drive robot (three-joint planar type, KOBELCO) and a PSD camera system to measure the position of the object as shown in Fig.8. Table 1 shows the link parameters of the robot. The task space is the horizontal plane and a LED is attached at a tip of a stick in order to represent the point object, where the measurement error is less than ± 3 mm in the task space. The computation of the control law is performed by using four CPUs (Transputer, T800, 25MHz).

The end-effector impedance of the robot is M_e = diag.[25, 25] kg, B_e = diag.[200, 200] Ns/m, K_e = diag.[400, 400] N/m; and the desired end-effector position is chosen as its initial position $X_d = [0.4, 0]^T$ m, where the initial posture is $\theta(0) = [0.8, -1.02, -1.49]^T$ rad.

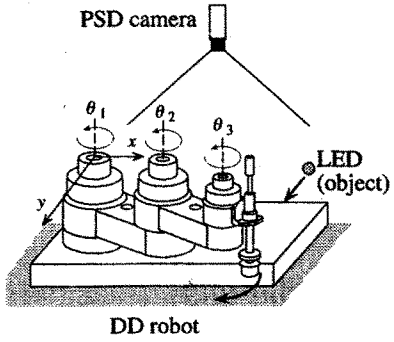

Figure 8: Experimental apparatus

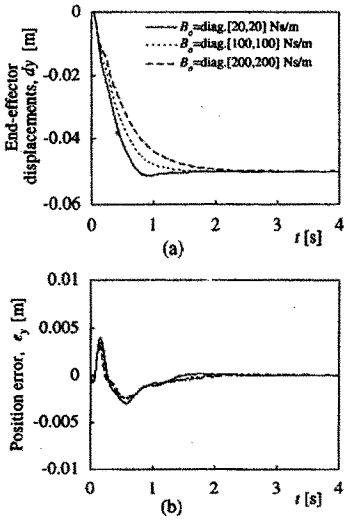

Figure 9: Step responses of the end-effector under the proposed method

The virtual circle with its radius $r = 0.3$ m is used, and the step responses of the end-effector are examined, where the object is located at the position with a distance 0.2 m apart from the initial position of the end-effector in the direction of y axis. Figure 9 (a) shows the experimental results of the step responses, where the virtual viscosity B_o is changed as B_o = diag.[20, 20], diag.[100, 100], diag.[200, 200] Ns/m with constant inertia and stiffness M_o = diag.[4, 4] kg, K_o = diag.[400, 400] N/m. Also in Fig. 9 (b) the error $e_y(t)$ between the measured trajectory X and the ideal end-effector trajectory X_v computed from Fig. 2 are shown. The sampling time is 2.6 ms. The step response of the end-effector changes depending on B_o, and the control error is quite small.

Figure 10 shows the end-effector trajectory $X(t)$ for the moving object $X_o(t)$, where $r = 0.2$ m; M_o = diag.[4, 4] kg; B_o = diag.[80, 80] Ns/m; K_o = diag.[400,

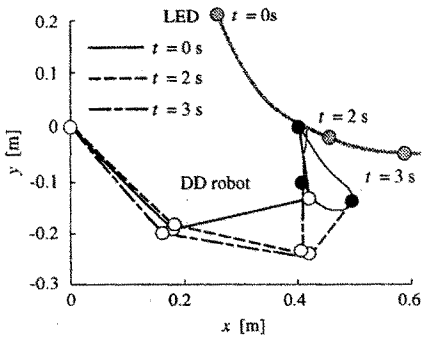

Figure 10: The DD robot avoiding the object

400] N/m. The posture of the robot changes according to the motion of the LED.

VI Conclusion

The present paper proposed the vision-based impedance control that can control the virtual impedance between the manipulator and the environment as well as the end-effector impedance. This method uses the virtual interaction force in order to express the relationship between the manipulator and the environment without contact, and the dynamics of the relative motion of the manipulator to the object can be regulated. The validity and feasibility were confirmed through the computer simulation and the robot experiments.

Generally speaking, there are many difficulties in vision-based robot control in 3D space such as measurements of 3D position of objects with occlusion, computational delay of the control system due to the video rate sampling. In the proposed method, however, visual information on the task space is required only for the interior of the virtual sphere. Therefore, instead of a visual sensor like a camera system, 3D position sensors such as a magnetic sensor and ultrasonic sensor can be used. Also, if the object is occluded by other object, the virtual impedance should be set to the occluding object.

Finally, the proposed method can be extended in order to deal with the interaction between the whole arm as well as the end-point of the manipulator and the environment [15].

References

[1] N.Hogan, "Impedance Control: An Approach to Manipulation, Parts I, II, III," ASME journal of Dynamic Systems, Measurement, and Control, 107, 1, pp.1–24, 1985.

[2] N. Hogan, "Stable Execution of Contact Tasks Using Impedance Control," Proc. of IEEE International Conference on Robotics and Automation, pp.1047–1054, 1987.

[3] S. Tachi, T. Sakaki, H. Arai, S. Nishizawa and J. F. Pelaez-Polo, "Impedance Control of a Direct-Drive Manipulator without Using Force Sensors," Advanced Robotics, vol.5, no.2, pp.183-205, 1991.

[4] E. Colgate and N. Hogan, "An Analysis of Contact Instability in terms of Passive Physical Equivalents," Proc. of IEEE International Conference on Robotics and Automation, pp.404–409, 1989.

[5] J. E. Agapakis, J. M. Katz, J. M. Friedman and G. N. Epstein, "Vision-aided Robotic Welding: An Approach and a Flexible Implementation," International Journal of Robotics Research, vol.9, no.5, pp.17–33, 1990.

[6] B. Espiau, F. Chaumette and P. Rives, "A new approach to visual servoing in robotics," IEEE Trans. on Robotics and Automation, vol.8, no.3, pp.313–326,1992.

[7] R. Sharma, J. -Y. Herve and P. Cucka, "Dynamic robot Manipulation Using Visual Tracking," in Proc. of IEEE International Conference on Robotics and Automation, vol. pp.1844–1849, 1992.

[8] A. Castano and S. Hutchinson "Visual Compliance: Task-Directed Visual Servo Control," IEEE Trans. on Robotics and Automation, vol.10, no.3, pp.334–342, 1994.

[9] T. Arai, H. Ogata and T. Suzuki, "Collision Avoidance Among Multiple Robots Using Virtual Impedance," Proc. of IEEE/RSJ International Workshop on Intelligent Robots and Systems, pp. 479–485, 1989.

[10] Y. Nakabo, I. Ishii and M. Ishikawa, "Robot Control Using Visual Impedance," Proc. of JSME Annual Conference on Robotics and Mechatronics '96, Vol.B, pp.999–1002, 1996. (In Japanese)

[11] M. Hatagi, H. Akamatsu, T. Tsuji and M. Kaneko, "Non-Contact Impedance Control for Manipulators," Proc. of JSME Annual Conference on Robotics and Mechatronics '96, Vol.B, pp.853–856, 1996.(In Japanese)

[12] O. Khatib, "A Unified approach for motion and force control of robot manipulators: the operational space formulation," IEEE J. of Robotics and Automation, vol.RA-3, no.1, pp.43-53, 1987.

[13] O. Khatib, "Motion/Force Redundancy of Manipulators," Proc. of Japan-U.S.A. Symposium on Flexible Automation, 1, pp.337-342, 1990.

[14] V. Potkonjak and M. Vukobtatovic, "Two New Methods for Computer Forming of Dynamic Equation of Active Mechanisms," Mechanism and Machine Theory, vol.14, no.3, pp.189–200, 1987.

[15] T. Tsuji, H. Akamatsu and M. Kaneko, "Non-Contact Impedance Control for Redundant Manipulators," Proc. of 1997 IEEE International Conference on Robotics and Automation, 1997 (in press).